

High critical current density $\text{YBa}_2\text{Cu}_3\text{O}_{7-\delta}$ thin films fabricated by *ex situ* processing at low pressures

Y Zhang^{1,2}, R Feenstra¹, J R Thompson^{1,3}, A A Gapud¹, T Aytug¹,
P M Martin⁴ and D K Christen¹

¹ Condensed Matter Sciences Division, Oak Ridge National Laboratory, Oak Ridge,
TN 37831, USA

² Department of Materials Science and Engineering, The University of Tennessee, Knoxville,
TN 37996, USA

³ Department of Physics and Astronomy, The University of Tennessee, Knoxville,
TN 37996, USA

⁴ Metals and Ceramics Division, Oak Ridge National Laboratory, Oak Ridge,
TN 37831, USA

Received 27 March 2004

Published 26 July 2004

Online at stacks.iop.org/SUST/17/1154

doi:10.1088/0953-2048/17/10/012

Abstract

There is interest in probing the feasibility and possible advantages of making uniform and cost-effective long-length coated conductors through a low-pressure processing approach. The low-pressure approach, eliminating the boundary layer and gas flow considerations, consumes much less of the processing gases and offers the possibility of improved uniformity and faster growth rate of superconducting films. Here, we have fabricated $\text{YBa}_2\text{Cu}_3\text{O}_{7-\delta}$ (YBCO) epitaxial films of thickness 0.1–1.0 μm on SrTiO_3 single crystal substrates using *ex situ* post-deposition processing of co-evaporated Y, BaF_2 and Cu precursors in a controlled low-pressure gas mixture of oxygen and water vapour. Partial pressures of oxygen (P_{O_2}) and water vapour ($P_{\text{H}_2\text{O}}$) as low as 10 and 0.1 mTorr, respectively, were used. X-ray diffraction and scanning electron microscopy inspection were conducted for structure characterization of the films. High critical current densities (J_c) of $\sim 3.6 \text{ MA cm}^{-2}$ at 77 K in self-field were obtained, yielding properties comparable to those of *in situ* films and *ex situ* films processed under atmospheric pressure condition.

1. Introduction

Ex situ synthesis of YBCO coatings is a promising method for fabricating YBCO coated conductors for large-scale applications. In these processes, physical vapour deposited (PVD) BaF_2 precursors or metal-organic deposited (MOD) trifluoroacetate (TFA) precursors are annealed to form epitaxial YBCO films on various substrates, including single crystals and buffered alloy tapes [1–4]. The post-deposition annealing is usually conducted at atmospheric pressure under a flowing gas mixture of oxygen, water vapour, and a carrier gas of nitrogen or argon. In recent years, considerable efforts have been devoted to better understanding the reaction mechanism and to optimize the processing [5–8].

For both PVD and MOD precursors, barium exists in a molecular state as BaF_2 . The epitaxial nucleation and growth of YBCO during the processing anneal is directly related to the decomposition of BaF_2 , i.e., according to the effective reaction

$$\frac{1}{2}\text{Y}_2\text{O}_3 + 2\text{BaF}_2 + 2\text{CuO} + \frac{1}{2}\text{Cu}_2\text{O} + 2\text{H}_2\text{O} \rightarrow \text{YBa}_2\text{Cu}_3\text{O}_{6.0} + 4\text{HF}. \quad (1)$$

Under typical atmospheric pressure processing conditions, removal of the decomposition product HF occurs by convection that is controlled by the gas flow conditions of particular reaction furnace geometry. For large area samples, an HF partial pressure gradient may form along the gas flow direction, leading potentially to non-uniform reaction and inhomogeneous films with poor properties [9]. Such a problem

may be ameliorated by a combination of increased gas flow rate and design of the processing furnace configuration. For large-area tape production, however, atmospheric pressure processing generally consumes large quantities of gases.

To obtain high critical current density (J_c) films, the post-annealing has to be well controlled to produce epitaxial c -axis oriented YBCO, with little nucleation and growth of a -axis and randomly oriented material. A rapid effective growth rate is also important for the practical production by either batch or reel-to-reel processes, particularly when thicker ($>1 \mu\text{m}$) films are concerned. In principle, a faster growth rate can be achieved by increasing the water partial pressure and/or reducing the HF partial pressure according to the reaction equation. By substantially reducing the total pressure (P_{tot}), the removal of HF can be greatly enhanced through rapid molecular diffusion instead of unduly relying on convection. Recently, it has been shown that, for TFA precursors, effective YBCO growth rates can be as rapid as 6 nm s^{-1} when the total pressure is reduced to about 1 Torr [10]. For co-evaporated BaF_2 precursors, an increased growth rate has also been observed under low total pressure of about 200 mTorr to 10 Torr [8, 11]. However, in the latter case the average growth rate was limited to about $0.2\text{--}0.3 \text{ nm s}^{-1}$ due to the formation of non- c -axis components that degrade the transport properties.

In this study, we focused on the possibility of fabricating YBCO thin films by *ex situ* processing under low pressures, and the influence of the basic annealing parameters on the properties of the films. The results envision a possible low-pressure quasi-static batch processing approach for long-length coated conductors. The precursor films were deposited on (100) SrTiO_3 substrates by e-beam co-evaporation of Y, BaF_2 and Cu at room temperature [1]. The compositions of the precursor films were determined by Rutherford backscattering spectroscopy (RBS), and the final thickness was measured using a step-profilometer. Post-deposition anneals were carried out in an induction vacuum furnace in which P_{O_2} and $P_{\text{H}_2\text{O}}$ were carefully controlled and varied to different levels. X-ray diffraction (XRD) and scanning electron microscopy (SEM) were used for structure characterization and morphology inspection of the YBCO films. The normal state electronic and superconducting properties were measured using a SQUID magnetometer as well as a standard four-probe technique.

2. Experimental aspects

The configuration of the induction vacuum furnace system is schematically shown in figure 1. The sample is located at the centre of a quartz tube in which the base pressure is about 2×10^{-6} Torr and is 4×10^{-6} Torr at the functional conductance as described here. In operation, valve (1) is set to maintain a gas flow that is consistent with the controlled pressure in the quartz tube. The gas flow rate is about 0.3 sccm in this particular system during the annealing. Water vapour is introduced first by adjusting the variable leak valve (11), and the partial pressure ($P_{\text{H}_2\text{O}}$) is monitored by the ionization vacuum gauge (9) and the MicropoleTM model MPA6-7-2/65C RGA (Residual Gas Analysis) detector (3). Values of $P_{\text{H}_2\text{O}}$ were set at different fixed levels from 2×10^{-5} to 8×10^{-3} Torr. After the stabilization of $P_{\text{H}_2\text{O}}$, high

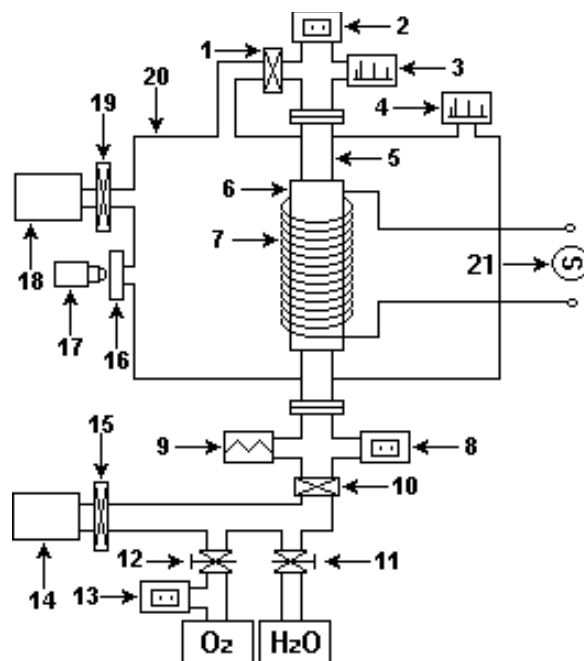


Figure 1. Schematic configuration of the post-annealing induction vacuum furnace system. 1, 10, 15—valves; 2, 8—convectron vacuum gauges; 3, 4—residual gas analyser (RGA) detectors; 5—quartz tube with sample inside; 6—susceptor; 7—induction coil; 9—ionization vacuum gauge; 11, 12—variable leak valves; 13—capacitance manometer; 14—roughing pump; 16—view port; 17—pyrometer; 18—cryopump; 19—gate valve; 20—UHV chamber; 21—RF generator.

purity oxygen is introduced by adjusting the variable leak valve (12). The total pressure in the quartz tube (P_{tot}) is set as indicated by the convectron vacuum gauges (2, 8), which are located upstream and downstream from the sample, respectively. Therefore, P_{O_2} is obtained as $P_{\text{O}_2} \approx P_{\text{tot}}$ when $P_{\text{H}_2\text{O}} \ll P_{\text{O}_2}$, and $P_{\text{O}_2} = P_{\text{tot}} - P_{\text{H}_2\text{O}}$ when $P_{\text{H}_2\text{O}}$ is comparable to P_{O_2} . For this study, all samples were annealed at a fixed temperature of $730 \text{ }^\circ\text{C}$. The sample temperature was monitored by a two-colour optical pyrometer (17) that was previously calibrated against a type-K thermocouple introduced at the sample position. The temperature ramp rate used for all anneals was about $60 \text{ }^\circ\text{C min}^{-1}$. Annealing times at $730 \text{ }^\circ\text{C}$ varied from 45 to 180 min, depending on film thickness. About 10 min before starting the cool down, the water vapour supply was shut off, and P_{O_2} was raised to 300 mTorr. The cooling rate was about $30 \text{ }^\circ\text{C min}^{-1}$, and upon reaching $450 \text{ }^\circ\text{C}$, more oxygen was introduced until $P_{\text{O}_2} = 150$ Torr, in order to oxygenate the YBCO.

To analyse the phases developed in the films, a Philips model XRG3100 x-ray diffractometer with $\text{Cu K}\alpha$ radiation was used to record powder $\theta\text{--}2\theta$ diffraction patterns. SEM micrographs were taken using a JEOL JSM-840 scanning electron microscope at a beam voltage of 7 kV. The electrical resistivity and critical current density (J_c) were measured using a standard four-probe method in which the J_c values were defined at a $1 \mu\text{V cm}^{-1}$ criterion. For films where the J_c values were measured by a Quantum Design MPMS 7 SQUID magnetometer, the magnetic fields were applied perpendicular to the film surfaces. In this case, the J_c values were determined by the application of the Bean critical state model formula,

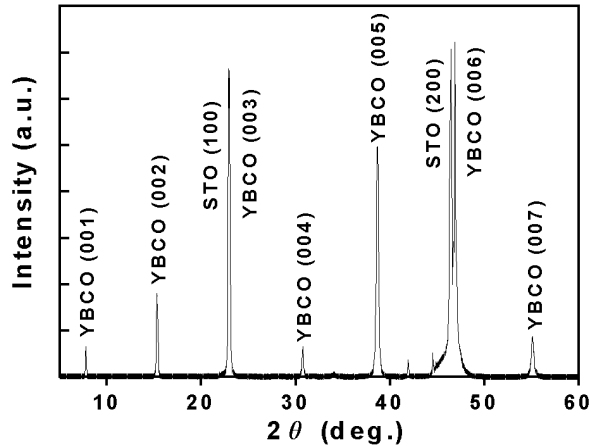


Figure 2. XRD θ - 2θ scan for a $0.34 \mu\text{m}$ thick sample annealed under $P_{\text{O}_2} = 10 \text{ mTorr}$ and $P_{\text{H}_2\text{O}} = 0.1 \text{ mTorr}$ at 730°C .

$J_c = 30\Delta M/d$, where ΔM is the magnetization hysteresis (emu cm^{-3}) and d is the lateral size of the sample (cm).

3. Results and discussion

YBCO films were obtained by post-annealing of the e-beam co-evaporated precursor films at different fixed P_{O_2} values of 10, 20, and 40 mTorr. The film thickness was either 0.14, 0.34 or $1.04 \mu\text{m}$. Figure 2 shows a typical XRD θ - 2θ scan obtained from a $0.34 \mu\text{m}$ thick sample that was annealed under $P_{\text{O}_2} = 10 \text{ mTorr}$ and $P_{\text{H}_2\text{O}} = 0.1 \text{ mTorr}$. Apparently, even at this low oxygen pressure, c -axis oriented YBCO film can be formed. XRD examination of other samples indicated that there is no appreciable difference in the phase composition and YBCO orientation as P_{O_2} is varied from 10 to 40 mTorr, with $P_{\text{H}_2\text{O}}$ fixed at 0.1 mTorr. However, when P_{O_2} was lowered to 2 mTorr, very little YBCO formed after a 90 min anneal. This result is consistent with extrapolation of the measured thermodynamic stability data [1]. It can be seen from the equilibrium phase diagram, figure 3, that the processing conditions used in this study are marginally within the YBCO stability region. By extension, we may speculate that c -axis YBCO films can be formed at lower P_{O_2} provided that the annealing temperature is lowered consistently with sufficient cation diffusion for phase formation.

The resistive superconducting transition of a $0.34 \mu\text{m}$ thick film processed at $P_{\text{O}_2} = 40 \text{ mTorr}$ and $P_{\text{H}_2\text{O}} = 0.1 \text{ mTorr}$ is shown in figure 4(a). It can be seen that the T_{co} is near 92 K and the transition width is around 1 K. Figure 4(b) compares the magnetic field dependence of transport J_c at 77 K of this sample with that of a typical *ex situ* film processed at 1 atm total pressure and a pulsed laser deposition (PLD) *in situ* film. It can be seen that their in-field behaviours are comparable. In this case, J_c at self-field for the sample annealed under low pressure is about 3.6 MA cm^{-2} ; this result is typical of the $3\text{--}4 \text{ MA cm}^{-2}$ J_c values obtained in this study for the samples processed at or near the optimal conditions. In figure 4(b), the self-field J_c values are 4.2 and 3.8 MA cm^{-2} for the atmospheric pressure annealed sample and the PLD sample, respectively. The decline in J_c with increasing magnetic field for the low-pressure processed film is somewhat less than that of the other two samples, and the irreversibility field, H_{irr} , is

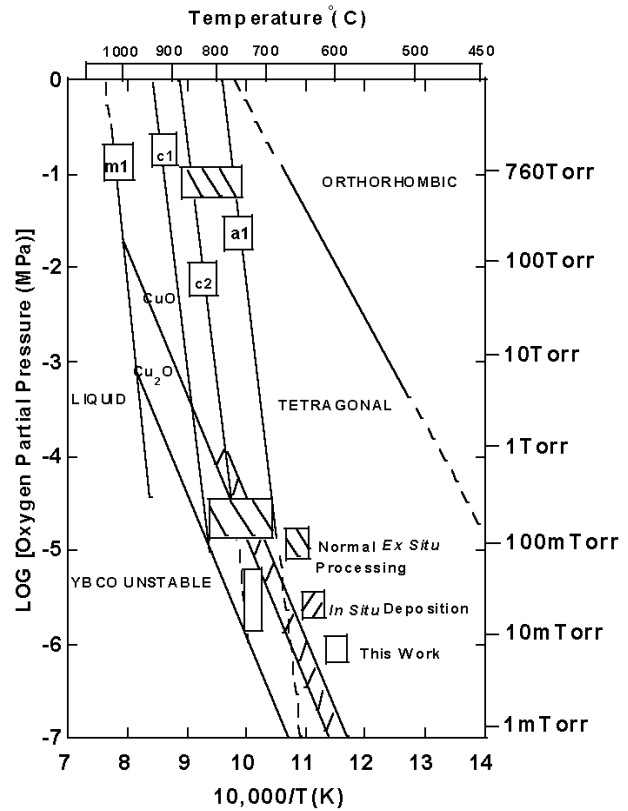


Figure 3. YBCO equilibrium phase diagram showing the low-pressure processing condition as well as the commonly used *ex situ* and *in situ* conditions for fabrication of YBCO films. It is generally believed that predominantly c -oriented films can be obtained between lines $c1$ and $c2$, and mixed c - and a -oriented films between $c2$ and $a1$; $m1$ is the melting line. The morphology lines are extrapolated to the low pressure regime of this study, where both fully c -oriented films and mixed c - and a -oriented films have been obtained. It is suggested that in addition to temperature and oxygen partial pressure P_{O_2} , the film orientation is also affected by other factors, such as the water partial pressure $P_{\text{H}_2\text{O}}$.

about 7.3 T, which is in the range for high performance YBCO on single crystal by any deposition process. Magnetization measurement of a $1.04 \mu\text{m}$ thick sample yields 77 K J_c values of 1.45 MA cm^{-2} at self-field and 0.2 MA cm^{-2} at 1 T. Figure 5 shows the magnetic field dependence of J_c at several different temperatures, determined from SQUID magnetometry measurements of another $0.34 \mu\text{m}$ thick sample annealed at $P_{\text{O}_2} = 40 \text{ mTorr}$ and $P_{\text{H}_2\text{O}} = 0.1 \text{ mTorr}$. Note that the agreement between transport and magnetization J_c measurements is good at low magnetic fields, whereas the magnetization measurements fall below those of transport at progressively higher fields and temperatures. This is due to the much lower effective voltage criterion of the magnetic measurement technique. In regimes of a shallow voltage-current relation, significant flux creep diminishes the magnetic hysteresis. At low fields, however, where the superconductor voltage-current relation is very sharp, large differences in voltage level have minimal effect on the deduced critical current.

In order to obtain fully c -axis oriented YBCO, the growth rate was controlled to be less than 0.2 nm s^{-1} by adjusting the water partial pressure to $\sim 0.1 \text{ mTorr}$. The preliminary

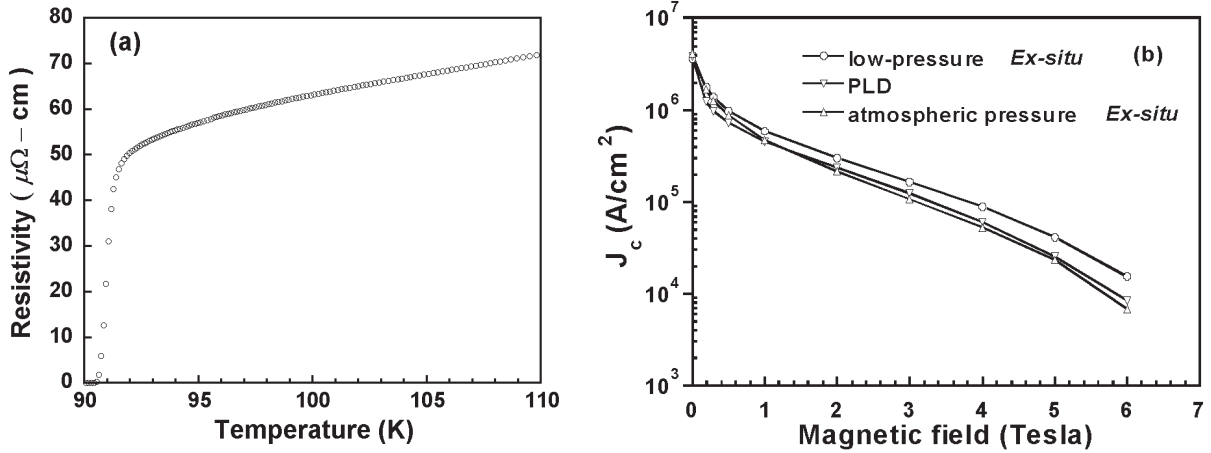


Figure 4. (a) Resistivity versus temperature and (b) magnetic field dependence of transport J_c values at 77 K for a $0.34 \mu\text{m}$ thick film annealed under $P_{\text{O}_2} = 40 \text{ mTorr}$ and $P_{\text{H}_2\text{O}} = 0.1 \text{ mTorr}$ at 730°C . Also shown in (b), for comparison, are the magnetic field dependences of J_c of an *ex situ* film processed under $P_{\text{O}_2} = 200 \text{ mTorr}$ in 1 atm total pressure and one by PLD *in situ* processing.

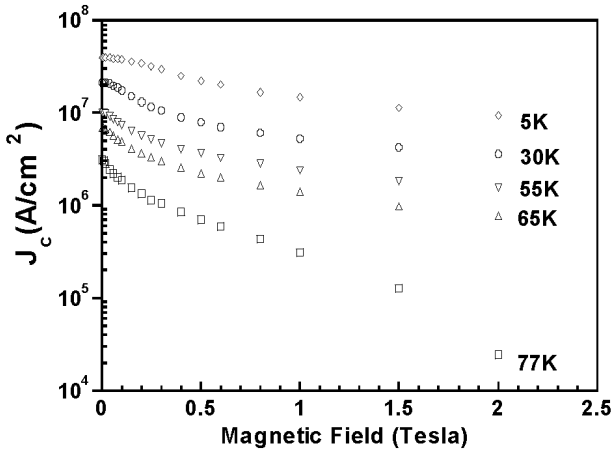


Figure 5. Magnetic field dependence of J_c values determined by magnetic hysteresis measurements at different temperatures for a $0.34 \mu\text{m}$ thick film annealed at $P_{\text{O}_2} = 40 \text{ mTorr}$ and $P_{\text{H}_2\text{O}} = 0.1 \text{ mTorr}$.

data indicate that, although this water partial pressure for low-pressure annealing is much lower than that used for atmospheric pressure processing, the YBCO growth rates are equivalent to those producing good *c*-axis films under atmospheric pressure. This result can be attributed to the much lower HF partial pressure at the sample surface under the low-pressure conditions, as we show with the following simple model.

The rate of the reaction (1), thus the YBCO film growth rate, strongly depends on the value of the ratio $P_{\text{HF}}^2/P_{\text{H}_2\text{O}}$. For this analysis, we assume that the concentrations of HF and H_2O at the reaction interface between precursor and YBCO can be approximated by the partial pressures P_{HF} and $P_{\text{H}_2\text{O}}$ at the sample surface [12]. In this approximation, the removal of HF determines the YBCO growth rate when the water partial pressure is maintained constant. When the total pressure is high, e.g. at 1 atmospheric pressure, the removal of HF at the surface is mainly implemented by gas flow (forced convection). At lower pressures, however, HF can diffuse from the surface more effectively, and the effect of HF removal on YBCO

growth rate can be evaluated in the absence of flow-related effects due to a large mean free path of gaseous molecules.

For an assumed constant YBCO growth-front rate, r (cm s^{-1}), the steady-state HF molecular out-flux, Φ ($\text{molecules cm}^{-2} \text{ s}^{-1}$) is

$$\Phi = \frac{4r}{V_{\text{cell}}}, \quad (2)$$

where $V_{\text{cell}} \cong 1.74 \times 10^{-22} \text{ cm}^3$, is the volume of the YBCO unit cell. For a planar geometry, the molecular flux of HF can be expressed as

$$\Phi = -D \frac{dC(z)}{dz}, \quad (3)$$

where D is the diffusivity of HF and $C(z)$ is the HF concentration, which can be related to P_{HF} as $C(0) = P_{\text{HF}}/kT$ at the sample surface.

From kinetic gas theory [13], the diffusivity D is inversely proportional to the total gas pressure, and for a binary gas system with HF as one component and the other gases (O_2 and H_2O) as the second component,

$$D \approx \frac{kT \sqrt{\frac{8kT}{\pi} \left(\frac{1}{M_{\text{HF}}} + \frac{1}{M_{\text{O}_2}} \right)}}{3\pi \delta^2 P_{\text{tot}}}, \quad (4)$$

where M_{HF} and M_{O_2} are the molecular weight of HF and O_2 , and $\delta = (\delta_{\text{HF}} + \delta_{\text{O}_2})/2$ is the average molecular diameter. For simplicity, suppose that the HF is absorbed at the wall of the furnace tube a distance z_0 away from the sample surface, so that $C(z_0) \approx 0$. Then, from equations (2)–(4), we obtain P_{HF} at the sample surface.

$$P_{\text{HF}} = \frac{12\pi r \delta^2 z_0 P_{\text{tot}}}{V_{\text{cell}} \sqrt{\frac{8kT}{\pi} \left(\frac{1}{M_{\text{HF}}} + \frac{1}{M_{\text{O}_2}} \right)}}. \quad (5)$$

Figure 6 gives the relationship between the ratio $P_{\text{HF}}/P_{\text{H}_2\text{O}}$ and the assumed YBCO growth rate r based on equation (5) for given total pressures and specific water partial pressures under typical atmospheric pressure processing and the present low-pressure processing conditions. It can be seen that,

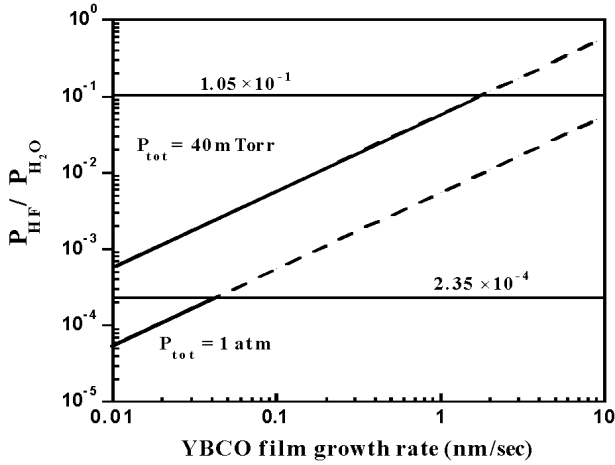


Figure 6. The inclined lines indicate the relationship, calculated according to equation (5), between $P_{\text{HF}}/P_{\text{H}_2\text{O}}$ and the YBCO growth rate r at given conditions of $P_{\text{tot}} = 1 \text{ atm}$ and $P_{\text{H}_2\text{O}} = 20 \text{ Torr}$ for atmospheric pressure processing, and $P_{\text{tot}} = 40 \text{ mTorr}$ and $P_{\text{H}_2\text{O}} = 0.1 \text{ mTorr}$ for low-pressure processing. Film growth cannot proceed above the horizontal lines given by the thermodynamic equilibrium ratios of $P_{\text{HF}}/P_{\text{H}_2\text{O}}$ calculated according to equation (6). The temperature used in the calculation was 730°C .

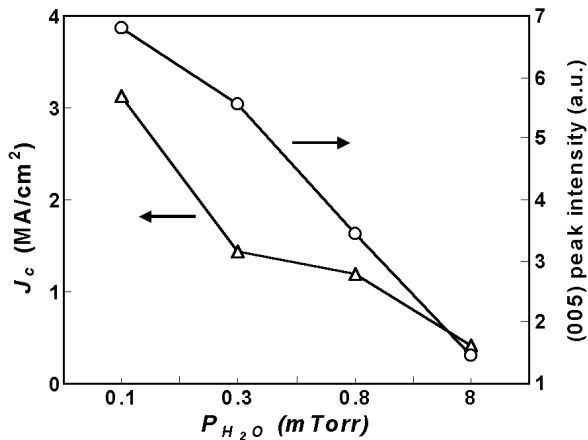


Figure 7. The dependence of J_c and the XRD θ - 2θ YBCO (005) peak intensities on the water vapour partial pressure $P_{\text{H}_2\text{O}}$, for $0.34 \mu\text{m}$ thick films processed at $P_{\text{O}_2} = 40 \text{ Torr}$.

in the absence of convection, the ratio $P_{\text{HF}}/P_{\text{H}_2\text{O}}$ for atmospheric pressure processing is lower than that for low-pressure processing at a given YBCO growth rate. However, the assumed growth rates r are only possible provided that the ratio $P_{\text{HF}}/P_{\text{H}_2\text{O}}$ is far below that defined by the thermodynamic equilibrium condition, when the Gibbs free energy of reaction (1) approaches zero, from which P_{HF} is calculated as

$$P_{\text{HF}} = \sqrt{P_{\text{H}_2\text{O}} \exp\left[-\frac{\Delta H^0 - T\Delta S^0}{2RT}\right]}, \quad (6)$$

where R is the gas constant. For reaction (1), the standard enthalpy $\Delta H^0 \cong 634 \text{ kJ mol}^{-1}$ and standard entropy $\Delta S^0 \cong 293 \text{ J mol}^{-1} \text{ K}^{-1}$, based on the data from [14] and [15]. At a temperature of 730°C , the calculated equilibrium ratios of $P_{\text{HF}}/P_{\text{H}_2\text{O}}$, which are also indicated in figure 6, are 2.35×10^{-4} and 1.05×10^{-1} for $P_{\text{H}_2\text{O}} = 20 \text{ Torr}$ and 0.1 mTorr ,

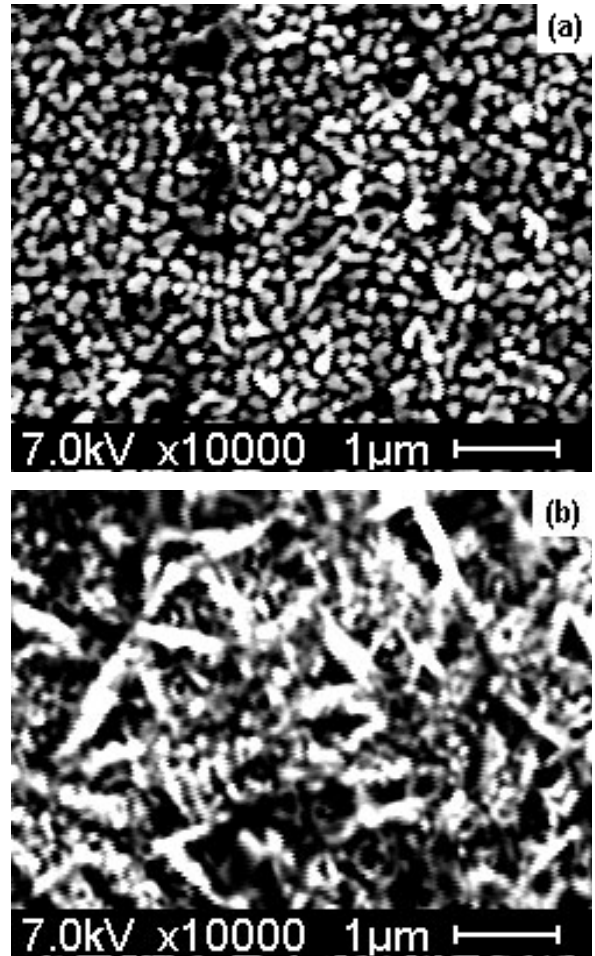


Figure 8. Surface SEM micrographs of films annealed at $P_{\text{O}_2} = 40 \text{ mTorr}$ and (a) $P_{\text{H}_2\text{O}} = 0.1 \text{ mTorr}$, (b) $P_{\text{H}_2\text{O}} = 0.8 \text{ mTorr}$. The difference indicates that the YBCO growth morphology is sensitive to the water partial pressure.

respectively. These ratios actually limit the validity of any assumed YBCO growth rates. It can be seen that without the forced gas flow, which should further decrease the ratio $P_{\text{HF}}/P_{\text{H}_2\text{O}}$, YBCO film growth is limited to a slower rate under atmospheric pressure processing conditions than for the low-pressure regime. In principle the experimentally observed rates of $r \geq 0.2 \text{ nm s}^{-1}$ for 1 atm processing are only possible with forced-flow convection.

To investigate the effect of $P_{\text{H}_2\text{O}}$ on YBCO formation, different $P_{\text{H}_2\text{O}}$ values ranging from 0.02 to 8 mTorr were used with P_{O_2} fixed at 40 mTorr . The XRD results indicated that YBCO was formed with complete c -axis orientation only at $P_{\text{H}_2\text{O}} \approx 0.1 \text{ mTorr}$. For all anneals with $P_{\text{H}_2\text{O}} > 0.1 \text{ mTorr}$, some a -axis and randomly oriented YBCO appeared along with the predominant c -axis YBCO. As $P_{\text{H}_2\text{O}}$ increases, the intensities of a -axis ($h00$) peaks and random crystalline peaks in the XRD θ - 2θ scan pattern increased, while the intensities of c -axis YBCO (001) peaks decreased. The qualitative relationship between the intensities of c -axis (005) peaks and the water partial pressures are shown in figure 7. Also shown are the J_c values at 77 K and self-field. The influence of water partial pressure on YBCO orientation can also be seen in the SEM surface morphology shown in figures 8(a)

and (b). Typical *c*-axis YBCO morphology is shown in figure 8(a), where the sample was annealed at $P_{\text{H}_2\text{O}} = 0.1$ mTorr. In contrast, randomly oriented YBCO is evident in figure 8(b), where $P_{\text{H}_2\text{O}} = 0.8$ mTorr. On the other hand, when the water partial pressure was lowered to about 0.02 mTorr, appreciable BaF_2 peaks appeared in the θ - 2θ scan, indicating an incomplete conversion. The results may explain the previous report [6] of low-pressure processing of BaF_2 precursors, where no additional water is introduced. In that case, we surmise that the furnace base pressure and degassed species were providing the necessary levels of H_2O .

4. Conclusion

YBCO films were successfully prepared by post-annealing of e-beam co-evaporated precursors under low oxygen pressure atmosphere. The highest J_c (77 K and self-field) obtained is 3.6 MA cm^{-2} for $0.34 \mu\text{m}$ thick films. Water is indispensable for the conversion reaction to proceed, although the water partial pressure used can be as low as 0.1 mTorr. The YBCO growth morphology is very sensitive to water partial pressure under the low-pressure condition we used. With increasing water partial pressure, the non-*c*-axis YBCO component increases, which results in the decrease of J_c values. Optimization of the YBCO growth rate, coupled with the suppression of non-*c*-axis growth, needs to be addressed in the future studies of these low-vacuum processing protocols.

Acknowledgments

This research is sponsored by the US Department of Energy, Office of Energy Efficiency and Renewable Energy, Office of Power Technologies, Superconductivity

Program under contract DE-AC05-00OR22725 with the Oak Ridge National Laboratory, managed by UT-Battelle, LLC.

References

- [1] Feenstra R, Lindemer T B, Budai J D and Galloway M D 1991 *J. Appl. Phys.* **69** 6569
- [2] Solovyov V F, Wiesmann H J, Suenaga M and Feenstra R 1998 *Physica C* **309** 269
- [3] Smith J A, Cima M J and Sonnenberg N 1999 *IEEE Trans. Appl. Supercond.* **9** 1531
- [4] Siegal M P, Clem P G, Dawley J T, Ong R J, Rodriguez M A and Overmyer D L 2002 *Appl. Phys. Lett.* **80** 2710
- [5] Solovyov V F, Wiesmann H J and Suenaga M 2003 *Supercond. Sci. Technol.* **16** L37
- [6] Ichinose A, Kiss T, Kikuchi A, Tachikawa K, Akita S and Inoue K 2003 *Supercond. Sci. Technol.* **16** 398
- [7] Teranishi R, Fuji H, Honjo T, Nakamura Y, Izumi T, Shiohara Y, Shibata J, Yamamoto T, Ikuhara Y and Yoshimura M 2002 *Physica C* **378–381** 1033
- [8] List F A, Specht E D, Heatherly L, Leonard K J, Sathyamurthy S and Kroeger D M 2003 *Physica C* **391** 350
- [9] Lee D F, List F A, Kroeger D M, Childs K W, O'Neill D and Robbins W B 2001 *Int. Workshop On Superconductivity Co-Sponsored By ISTE and MRS (Honolulu, Hawaii, 2001)* pp S3–4 (Program and Extended Abstracts)
- [10] Yoshizumi M, Seleznev I and Cima M J 2003 *Wire Development Workshop, USDOE Superconductivity Program for Electric Power (St Petersburg, FL, 2003)* unpublished
- [11] Suenaga M 2002 *Physica C* **378–381** 1045
- [12] Solovyov V F, Wiesmann H J, Wu L, Zhu Y and Suenaga M 2001 *IEEE Trans. Appl. Supercond.* **11** 2939
- [13] Dushman S 1960 *Scientific Foundations of Vacuum Technique* (New York: Wiley)
- [14] Lide D R 2002 *CRC Handbook of Chemistry and Physics* 83rd edn (Boca Raton, FL: CRC Press)
- [15] Idemoto Y, Takahashi J and Fueki K 1992 *Physica C* **194** 177